ADVANCES IN ATMOSPHERIC SCIENCES, VOL. 32, OCTOBER 2015, 1341–1353

Quantitative Analysis of the Feedback Induced by the Freshwater Flux in the Tropical Pacific Using CMIP5

ZHI Hai[1], ZHANG Rong-Hua*[2], LIN Pengfei[3], and WANG Lanning[4]

[1]*The Earth System Modeling Center and College of Atmospheric Sciences, Nanjing University of Information Science and Technology, Nanjing* 210044

[2]*Key Laboratory of Ocean Circulation and Waves, Institute of Oceanology, Chinese Academy of Sciences, Qingdao* 266071

[3]*State Key Laboratory of Numerical Modeling for Atmospheric Sciences and Geophysical Fluid Dynamics, Institute of Atmospheric Physics, Chinese Academy of Sciences, Beijing* 100029

[4]*College of Global Change and Earth System Science, Beijing Normal University, Beijing* 100875

(Received 9 March 2015; revised 17 April 2015; accepted 20 April 2015)

ABSTRACT

Freshwater flux (FWF) directly affects sea surface salinity (SSS) and hence modulates sea surface temperature (SST) in the tropical Pacific. This paper quantifies a positive correlation between FWF and SST using observations and simulations of the fifth phase of the Coupled Model Intercomparison Project (CMIP5) to analyze the interannual variability in the tropical Pacific. Comparisons among the displacements of FWF, SSS and SST interannual variabilities illustrate that a large FWF variability is located in the west-central equatorial Pacific, covarying with a large SSS variability, whereas a large SST variability is located in the eastern equatorial Pacific. Most CMIP5 models can reproduce the fact that FWF leads to positive feedback to SST through an SSS anomaly as observed. However, the difference in each model's performance results from different simulation capabilities of the CMIP5 models in the magnitudes and positions of the interannual variabilities, including the mixed layer depth and the buoyancy flux in the equatorial Pacific. SSS anomalies simulated from the CMIP5 multi-model are sensitive to FWF interannual anomalies, which can lead to differences in feedback to interannual SST variabilities. The relationships among the FWF, SSS and SST interannual variabilities can be derived using linear quantitative measures from observations and the CMIP5 multi-model simulations. A 1 mm d^{-1} FWF anomaly corresponds to an SSS anomaly of nearly 0.12 psu in the western tropical Pacific and a 0.11°C SST anomaly in the eastern tropical Pacific.

Key words: feedback, freshwater flux, CMIP5, correlation

Citation: Zhi, H., R.-H. Zhang, P. F. Lin, and L. N. Wang, 2015: Quantitative analysis of the feedback induced by the freshwater flux in the tropical Pacific using CMIP5. *Adv. Atmos. Sci.*, **32**(10), 1341–1353, doi: 10.1007/s00376-015-5064-0.

1. Introduction

Freshwater exchange at the atmosphere–ocean interface is one of the most important forcing conditions for both oceanic general circulation and the climate system. In particular, the freshwater flux (FWF), i.e., precipitation minus evaporation, is a key factor in controlling the salinity distribution and modulating thermohaline circulation (Huang et al., 2005). Forced by atmospheric fields, the oceanic changes can produce feedback to the atmosphere in which the important oceanic field affected is sea surface temperature (SST). In addition, different from ocean heat flux forcing, FWF forcing acts to drive a change in SST whereas the heat flux represents a passive response to SST change (Zhang and Busalacchi, 2009). The significance and implications of these relationships need to be investigated more thoroughly to understand the physical characteristics and to improve model simulations of the interannual variability in the tropical Pacific, particularly that associated with ENSO and its diversity (Zhang et al., 2013; Zheng et al., 2014).

Previous research has mainly focused on the effects of atmospheric forcing components of surface heat flux and winds in the tropical Pacific (e.g., Bjerknes, 1969; Meehl et al., 2001; Yu and Boer, 2002; Kim et al., 2007; Yu and Weller, 2007; Zhang et al., 2014). Recently, however, FWF forcing and its related salinity effects on climate variability have attracted great attention, and there has been significant progress in understanding the physical characteristics and modeling the roles of FWF forcing in climate variability (e.g., Zhang and Busalacchi, 2009; Zhang et al., 2010; Hackert et al., 2011; Ham et al., 2012; Wu et al., 2010; Zheng and Zhang, 2012; Zheng et al., 2014). These studies have demonstrated that FWF and its related salinity fields first affect the oceanic

* Corresponding author: ZHANG Rong-Hua
Email: rzhang@qdio.ac.cn

density gradients and stratification, and then have the ability to maintain the mean climate and its variability (e.g., Maes, 2000; Lagerloef, 2002; Curry et al., 2003; Boyer et al., 2005; Huang et al., 2005; Levitus et al., 2005; Ballabrera-Poy et al., 2007; Cravatte et al., 2009; Collins et al., 2010). For instance, sensitivity analyses following an introduction of FWF perturbation have revealed obvious effects on SSTs (Levitus, 1989; Delcroix and Hénin, 1991; Manabe and Stouffer, 1995; Béthoux et al., 1998; Maes, 1998; Wong et al., 1999, 2001; Dickson et al., 2002; Jacobs et al., 2002; Fedorov et al., 2004; Huang et al., 2005; Huang and Mehta, 2005; Ma et al., 2013). In considering the coupling between the ocean and atmosphere, some additional processes start to act because the FWF forcing-induced changes in SSTs can produce additional feedback to the atmosphere. Additionally, FWF affects the depth of the mixed layer through its direct contributions to the buoyancy flux (Q_B), which further causes the entrainment of subsurface water into the mixed layer.

The effect of FWF on ocean salinity and the transport of freshwater in the ocean are not thoroughly understood, and there are many unresolved questions remaining with regard to the tropical Pacific. For example, previous studies have tended to analyze the relationship of FWF feedback with related physical fields through diagnosing, instead of quantifying, the effects among these relationships. Additionally, model performances are strikingly different in representing the related feedbacks, with large uncertainty and biases. The released simulation results of phase 5 of the Coupled Model Intercomparison Project (CMIP5) experiments (Taylor et al., 2012) have provided a good opportunity to further explore FWF feedback to climate variability. Preliminary analyses indicate that interannual variability of FWF in the tropical Pacific bears a close relationship with SST associated with the evolution of ENSO (Zhang et al., 2012; Zheng and Zhang, 2012). Thus, interannual variabilities of FWF display a nonlocal positive relationship with SST during ENSO evolution. Accordingly, we can evaluate the FWF modulation of SST in coupled models to not only understand interannual anomalous signal mechanisms, but also to analyze FWF bias in the interannual variability simulated by the CMIP5 multi-model through assessing the feedback in the tropical Pacific. These CMIP5-based analyses support the view that FWF forcing and its related feedback should receive adequate attention due to its strong interannual anomalies related to ENSO.

The purpose of this study is to evaluate CMIP5 multi-model simulation performance with regard to the interannual variability of oceanic physical fields in the equatorial Pacific. In addition, FWF feedback to SST in the tropical Pacific is explored and FWF feedback to SST and related oceanic fields is quantified. A description of the multi-model, the observational and reanalysis data, and the definition and calculation used for Q_B are presented in section 2. In section 3, the positions and intensities in the interannual spatial distribution are compared. In section 4, multi-model simulations and observations of physical fields are compared, and the difference in the correlation between FWF and SST within the CMIP5 multi-model is explained by analyzing oceanic processes. The linear relationship induced for FWF and SST is qualitatively analyzed based on the differences within the CMIP5 models and observation in section 5. A summary and conclusion are provided in section 6.

2. Data and methodology

2.1. *CMIP5 multi-model data*

Data from the CMIP5 multi-model archive are used, which are available in the Program for Climate Model Diagnosis and Inter-comparison (PCMDI) Earth System Grid (ESG) (http://pcmdi3.llnl.gov/esgcet/). In the current study, we perform analyses using the 23 models listed in Table 1. We make use of Pre-industrial control (Pi-control) scenario simulations (Taylor et al., 2012) to analyze the following variables in the tropical Pacific: SST, precipitation, evaporation, and SSS. The first ensemble member is used where multiple ensemble members are available for any model. All CMIP5 data are interpolated to a $1^\circ \times 1^\circ$ resolution global grid to compare the data. In this paper, data from the last 100 years for the 23 Pi-control models are selected to focus on climate characteristics and variability. Unless stated otherwise, Pi-control simulations are compared in the period 1909–2008 (100 yr).

2.2. *Observational and reanalysis data*

To compare with CMIP5 multi-model simulations, we use the following datasets. The observed precipitation data are from version 2 of the Global Precipitation Climatology Project (GPCP) dataset, covering 1979–2013, with a $2.5^\circ \times 2.5^\circ$ horizontal resolution (Adler et al., 2003). Evaporation is derived from the Objectively Analyzed Air–Sea Fluxes (OAFlux; Yu and Weller, 2007). Net heat flux data of monthly and long-term climatology fields at the sea surface (latent and sensible heat fluxes and flux-related surface meteorology) are derived from the OAFlux data from 1958 to present (1° gridded) and the surface radiation data from the International Satellite Cloud Climatology Project from 1983 to 2009 (resolution: 2.5°) (Schiffer and Rossow, 1985). Monthly mixed layer depth (MLD) data and its climatological fields are directly available from the International Pacific Research Center/Asia-Pacific Data-Research Center Argo products, which cover the period from 2005 to 2013. SST data are from version 3b of the Extended Reconstructed Sea Surface Temperature (ERSST) dataset, which includes SST data from January 1854 to the present day (Smith et al., 2008). SSS data are from the quality-controlled subsurface ocean temperature and salinity data of the Met Office Hadley Centre observation datasets, which are available from 1950 to the present day and provide separate files for each month (Ingleby and Huddleston, 2007). Trends for all of the above data are removed to eliminate the response to global warming and the data are interpolated to a $1^\circ \times 1^\circ$ resolution global grid.

Table 1. List of the CMIP5 models used for the Pi-control scenario study.

No.	Model	Atmosphere Resolution (°) (lon × lat)	Atmosphere Levels	Ocean Resolution (°) (lon × lat)	Ocean Levels	Run span	Reference
1	Australian Community Climate and Earth-System Simulator (ACCESS), ACCESS version 1.3 (ACCESS1.3)	1.875 × 1.25	L38	1.0 × 1.0	L50	559	Dix et al. (2013)
2	Beijing Normal University–Earth System Model (BNU-ESM)	2.8 × 2.8	L17	1.0 × 1.0	L50	1050	Ji et al. (2014)
3	Community Climate System Model, version 4 (CCSM4)	1.25 × 1.25	L17	1.0 × 0.5	L60	320	Danabasoglu et al. (2012)
4	CESM, version 1, using Community Atmosphere Model (CAM), version 5 (CESM1-CAM5)	1.25 × 1.25	L17	1.0 × 1.0	L60	277	Meehl et al. (2013)
5	Centro Euro-Mediterraneo sui Cambiamenti Climatici(CMCC) Carbon Earth System-Model (CMCC-CESM)	3.75 × 3.75	L39	2.0 × 2.0	L31	850	http://www.cmcc.it/datamodels/models
6	Centre National de Recherches Meteorologiques Coupled Global Climate Model, version 5 (CNRM-CM5)	1.4 × 1.4	L31	1.0 × 1.0	L42	500	Voldoire et al. (2013)
7	Commonwealth Scientific and Industrial Research Organisation Mark, version 3.6.0 (CSIRO Mk3.6.0)	1.875 × 1.875	L18	1.875 × 0.94	L31	996	Jeffrey et al. (2013)
8	Flexible Global Ocean–Atmosphere–Land System Model (FGOALS), Grid point version 2 (FGOALS-g2)	3.0 × 2.8	L26	1.0 × 1.0	L30	900	Li et al. (2013)
9	FGOALS, second spectral versio (FGOALS-s2)	2.8 × 1.7	L26	0.5 × 0.5	L30	500	Bao et al. (2013)
10	Geophysical Fluid Dynamics Laboratory (GFDL) Climate Model, version 3 (GFDL CM3)	2.5 × 2.0	L48	1.0 × 1.0	L50	500	Griffies et al. (2011)
11	GFDL Earth System Model with Generalized Ocean Layer Dynamics (GOLD) component (GFDL-ESM2G)	2.5 × 2.0	L24	1.0 × 1.0	L63	400	Dunne et al. (2013)
12	GFDL Earth System Model with Modular Ocean Model, version 4 (GFDL-ESM2M)	2.5 × 2.0	L24	1.0 × 1.0	L50	300	Dunne et al. (2013)
13	Hadley Centre Coupled Model,version 3 (HadCM3)	3.75 × 2.5	L19	1.25 × 1.25	L20	670	Collins et al. (2001)
14	HadGEM, version 2–Earth System (HadGEM2-ES)	1.875 × 1.25	L38	1.0 × 1.0	L40	1000	Jones et al. (2011)
15	L'Institut Pierre-Simon Laplace (IPSL) Coupled Model, version 5A, low resolution (IPSL-CM5A-LR)	2.5 × 1.25	L39	2.0 × 2.0	L31	500	Dufresne et al. (2013)
16	L'Institut Pierre-Simon Laplace IPSL Coupled Model, version 5A, mid resolution (IPSL-CM5A-MR)	2.5 × 1.25	L39	2.0 × 2.0	L31	500	Dufresne et al. (2013)
17	Model for Interdisciplinary Research on Climate (MIROC), MIROC, version 5 (MIROC5)	1.4 × 1.4	L40	1.4 × 1.0	L50	559	Watanabe et al. (2010)
18	Max Planck Institute (MPI) Earth System Model, low resolution (MPI-ESM-LR)	1.875 × 1.875	L47	1.5 × 1.5	L40	500	Giorgetta et al. (2013)
19	MPI Earth System Model, paleo(MPI-ESM-P)	1.875 × 1.875	L47	1.5 × 1.5	L40	1050	Giorgetta et al. (2013)
20	MPI Earth System Model, medium resolution (MPI-ESM-MR)	1.875 × 1.875	L47	1.5 × 1.5	L40	320	Giorgetta et al. (2013)
21	Meteorological Research Institute Coupled Atmosphere–Ocean General Circulation Model, version 3 (MRI-CGCM3)	0.75 × 0.75	L48	1.0 × 0.5	L51	277	Yukimoto et al. (2012)
22	Norwegian Earth System Model (NorESM), version 1 (intermediate resolution) (NorESM1-M)	2.5 × 1.9	L26	1.0 × 1.0	L53	850	Bentsen et al. (2012); Iversen et al. (2013)
23	Beijing Climate Center (BCC), Climate System Model, version 1.1 (BCC-CSM1.1)	2.8 × 2.8	L26	1.0 × 1.0	L40	500	Wu et al. (2014)

2.3. *Buoyancy flux*

The Q_B field, together with wind and heat flux, controls the formation of MLD, which affects the entrainment of subsurface cold water into the upper surface in the equatorial Pacific. The Q_B at the sea surface can be defined as (Zhang et al., 2010)

$$Q_B = \frac{\alpha \text{HF}}{(\rho c_p)} + \beta S_0 \text{FWF} = Q_T + Q_S \ , \quad (1)$$

where HF is the net heat flux at the sea surface (positive when the ocean is receiving heat flux); FWF ($= P - E$, where P is precipitation and E is evaporation) is the net freshwater flux (when the ocean is gaining net freshwater, FWF is positive); α is the thermal expansion coefficient; β the haline contraction coefficient; S_0 the reference surface salinity; c_p the heat capacity of seawater, and ρ the density of seawater. The surface Q_B is the net contribution of the HF part (Q_T) and the FWF part (Q_S).

3. Spatial distributions of interannual variability

Zhang and Busalacchi (2009) indicated that SST anomalies generated by ENSO induce large nonlocal anomalous FWF variability over the western and central Pacific, which directly affects SSS, leading to changes in oceanic processes, and enhances the SST anomalies. Figure 1 shows the FWF interannual standard deviation (STD) of the CMIP5 multi-model and observations in the tropical Pacific. It can be seen that a large FWF variability (larger than 2.5 mm d^{-1}) is located in the west-central equatorial Pacific and in the South Pacific Convergence Zone (SPCZ), which extends southeastward in the South Pacific Ocean, with a maximum FWF variability of more than 4.0 mm d^{-1} from 160°–180°W in the west-central equatorial Pacific. The distribution of FWF interannual variability indicates that FWF displacement is similar to the precipitation pattern in tropical regions, such as the intertropical convergence zone (ITCZ). Hence, precipitation interannual variability is a primary factor leading to FWF anomalies in the equatorial Pacific.

FWF variability caused by a precipitation anomaly in the equatorial Pacific leads to a response in the local anomalous ocean physics, in which fresh water gained and lost in the ocean can directly lead to a change in salinity at the surface layer. The spatial distribution of SSS interannual anomalous STDs simulated by the multi-model and from observations is shown in Fig. 2. A large SSS variability (larger than 2.5 psu), covarying with the large FWF variability, is found in the

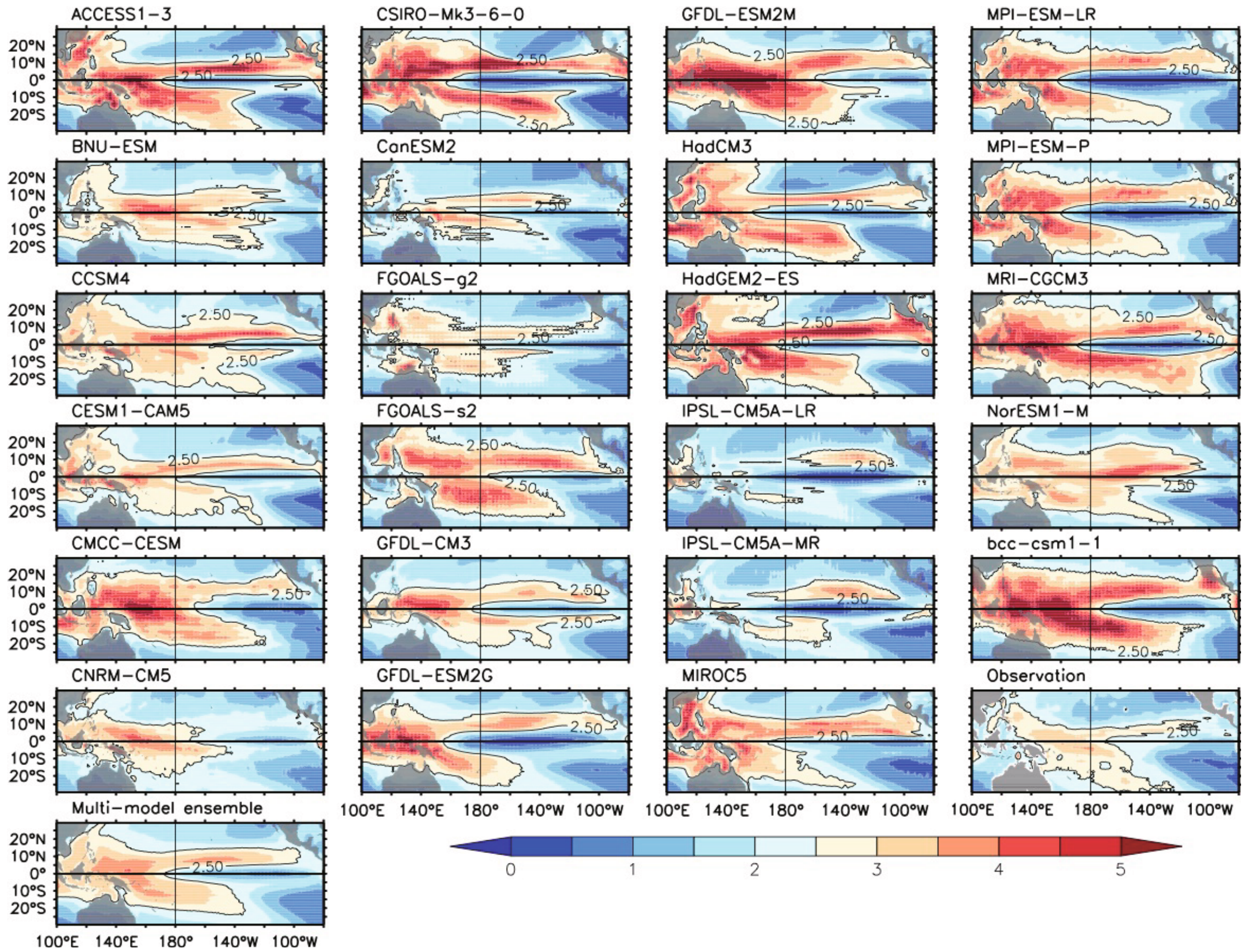

Fig. 1. STD of FWF calculated from the results of the CMIP5 multi-model simulations and based on observations (right of the bottom panel) in the tropical Pacific. Units: mm d^{-1}.

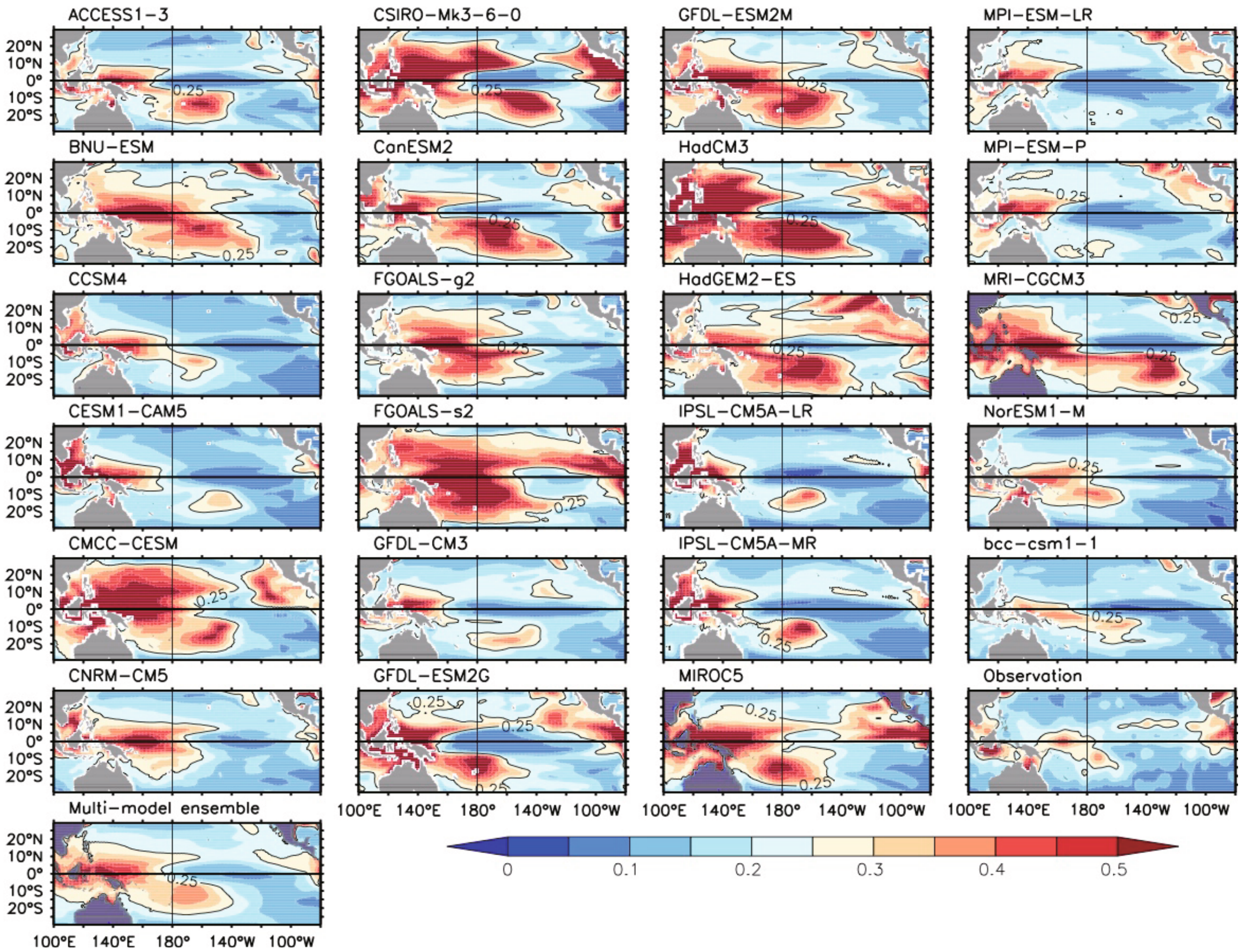

Fig. 2. STD of SSS calculated from the results of the CMIP5 multi-model simulations and based on observations (right of the bottom panel) in the tropical Pacific. Units: psu.

western tropical Pacific based on observations. High salinity is located in the subtropical convergence zone of the Northern Hemisphere and extends eastward across the date line, with a maximum FWF variability of more than 0.5 psu between 160°W and 180°W in the west-central equatorial Pacific. It is confirmed that FWF is the main factor responsible for SSS change in the equatorial Pacific, where the evaluation of the sensitivity of precipitation was also conducted to assess the possible impact of salinity on the tropical Pacific climate variability.

Most models (21 out of the 23) agree well with observations in terms of the distribution of interannual FWF (Fig. 1) and SSS (Fig. 2) variability. As shown in Fig. 1, most of the CMIP5 multi-models (all except two: IPSL-CM5A-LR and IPSL-CM5A-MR) show large FWF variability in the west-central Pacific. However, 10 of the 21/23 models that have a large variability in the equatorial region illustrate weaker interannual variability, with a large variability located farther west than observed, and west of the date line. The amplitude of variation for most models (17 of 23), 5.0 mm d^{-1} on average, is larger than that of observations.

Not only can the multi-model simulate the interannual FWF feature observed in the tropical Pacific, but it can also reflect the FWF sensitivity to precipitation contributions, which is the primary controlling factor of FWF interannual variability. Moreover, precipitation is the primary factor causing the difference of FWF anomalous patterns simulated by coupled models (Kang et al., 2014).

Furthermore, the corresponding SSS distribution simulated by the CMIP5 multi-model shows the observed feature of a large SSS interannual variability [large than 3.5 psu (Practical salinity units: ‰)] located in the west-central equatorial Pacific. The amplitudes of the interannual variabilities of most CMIP5 multi-models are greater than that in observations and the areas of the large variabilities are commonly greater than that observed. In addition, a difference among CMIP5 multi-models exists in the locations of large variabilities. For example, some models (9 of 23) extend across the date line, but others (14 of 23) are west of the date line. With the eastern front of a large SSS variability simulated from the multi-model moving near the date line, the eastern borders of the large variabilities of most models (16 of 23) move eastward across the date line. SSS variabilities of some models (7 of 23) are weaker and are located in the west equatorial Pacific, where the displacement of large variabilities are farther west than observed. For example, the weaker FWF interannual variability of IPSL-CM5A-MR leads to a smaller SSS anomaly. By contrast, the stronger FWF interannual change of CMCC-CESM corresponds to a larger variability of SSS.

FWF directly affects SSS and changes the upper ocean density so that the ocean physical fields have a positive feedback to SST anomalies in the equatorial Pacific. Figure 3 shows the STD distribution of an SST anomaly in the equatorial Pacific, which is the same as the feature of the observed ENSO pattern. A large SST variability (larger than 0.8°C) is located in the eastern tropical Pacific, and the area of large variability extends westward along the equator and is near the date line.

Figure 3 shows that the large SST variabilities simulated by most models are located in the east-central Pacific, but the interannual SST variabilities simulated by the multi-model show the difference in the location and intensity of the larger variability. The large SST variabilities of some models (13 of 23) are located westward, across the date line, with a stronger SST variability than that observed.

Based on the above assessment of the spatial distribution, it is evident that most of the CMIP5 multi-models can reproduce the corresponding spatial pattern of FWF, SSS and SST, in which a large FWF–SSS variability is located in the west-central equatorial Pacific and an SST anomaly is located in the east-central equatorial Pacific. It is demonstrated that inherent relationships can be clearly observed among the interannual variabilities of FWF, SSS and SST simulated by the CMIP5 multi-model. Regarding the differences shown by model simulations and observations, the spatial distribution and the magnitude of interannual variabilities are completely inconsistent. For example, in the west-central Pacific, the stronger FWF variability, covarying with the stronger SSS, corresponds to a higher SST interannual anomaly in the east-central Pacific and vice versa for the weaker interannual variabilities of FWF, SSS and SST.

4. Contrast in the physical processes between the CMIP5 multi-model and observations

The CMIP5 multi-model can satisfactorily represent FWF feedback effects on SST in the tropical Pacific, for which Zhang et al. (2010) and Zheng and Zhang (2012) have carried out detailed analysis and diagnosis. The effect of FWF on this feedback process is further verified by the observed interannual variability and CMIP5 multi-model simulations.

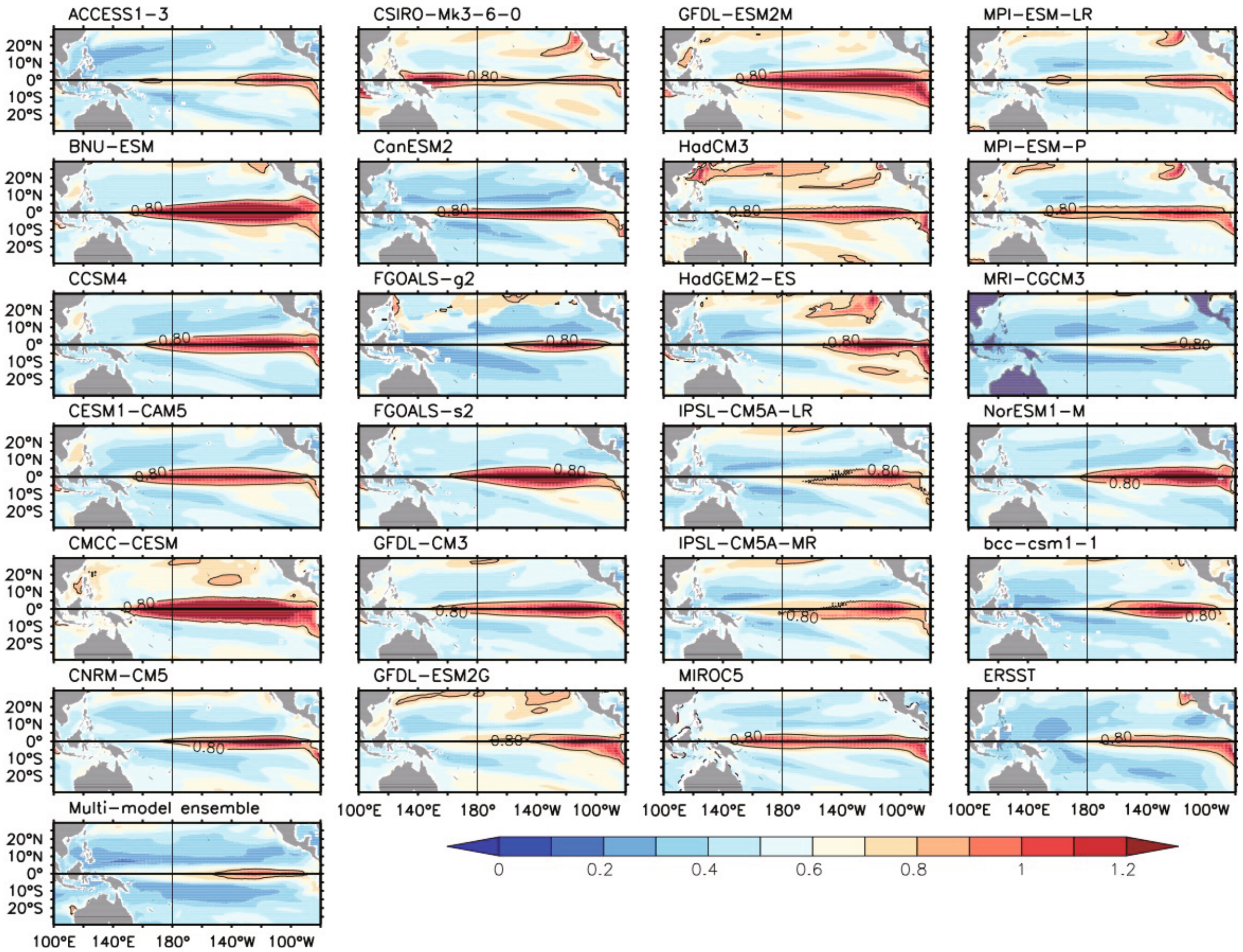

Fig. 3. STD of SST calculated from the results of the CMIP5 multi-model simulations and based on ERSST (right of the bottom panels) in the tropical Pacific. Units: °C.

FWF affects SSS anomalies directly and then modulates other fields, such as MLD and Q_B. Relationships among these interannual ocean variabilities have been discussed previously (Zhang and Busalacchi, 2009; Zheng and Zhang, 2012), and it has been shown that the effect induced by FWF on the related physical fields associated with ENSO evolution is the intrinsic linkage between FWF and SSS, and MLD and Q_B.

The FWF forcing in the equatorial Pacific tends to indirectly modulate SST conditions in two ways (Zhang et al., 2010). First, during El Niño, FWF into the ocean surface acts to decrease the salinity in the west-central region where the SST is relatively high. The decreased salinity acts to stabilize the upper ocean and suppress the vertical mixing at the base of the mixed layer. Secondly, the FWF into the ocean has a direct effect on Q_B, which in turn exerts an influence on MLD and the entrainment of subsurface water at the base of the mixing layer. Because Q_T and Q_S are negatively correlated during ENSO cycles, their effects on Q_B tend to compensate for one another. Thus, as part of Q_B, the FWF into the ocean acts to compensate for the Q_T, leading to a smaller negative Q_B. The reduced negative Q_B tends to decrease MLD, and FWF into the ocean induces oceanic processes that lead to a less pronounced cooling effect on the surface layers in the west-central basin, which in turn acts to enhance the warming conditions during El Niño, indicating a positive feedback to SST. Therefore, MLD and Q_B are two important physical fields in FWF feedback to SST in the equatorial Pacific.

To more clearly identify the relationships between interannual anomalies of various oceanic variables and SST, the GFDL-ESM2M model is selected because of its relatively better performance. Then, a regression analysis is conducted along the equator for interannual anomalies of SST, SSS, MLD, and the buoyancy flux components (i.e., Q_B, Q_T and Q_S) during ENSO. The dominant pattern for interannual SST

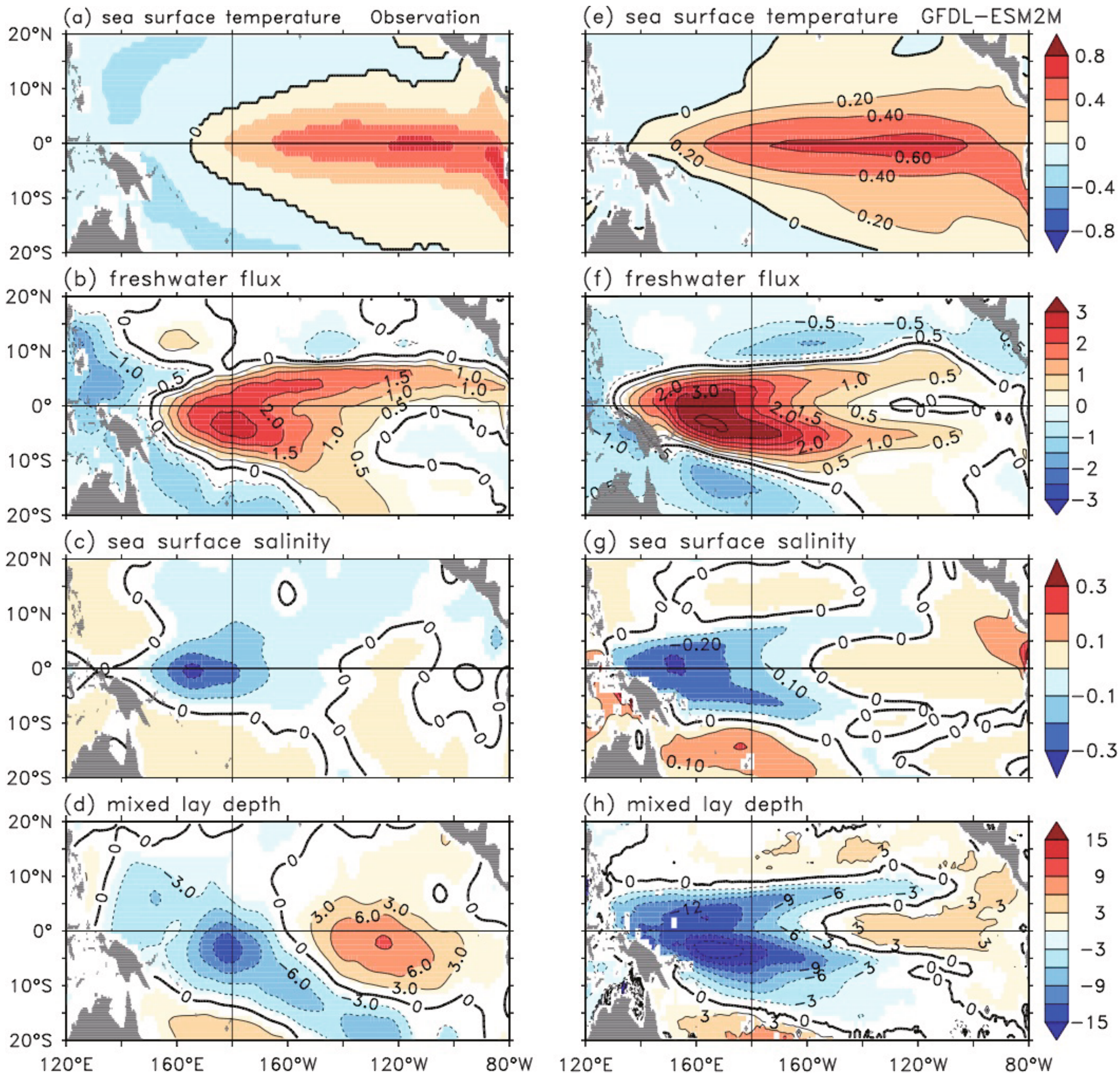

Fig. 4. SST EOF1 spatial pattern and the regressive spatial patterns from SST PC1 in the equatorial Pacific: (a) SST EOF1, (b) FWF, (c) SSS, (d) MLD with observation; (e) SST EOF1, (f) FWF, (g) SSS, (h) MLD simulated by GFDL-ESM2M. The units are °C for SST, 1.0×10^{-5} kg m^{-2} s^{-1} (°C)$^{-1}$ for FWF, psu (°C)$^{-1}$ for SSS, and m (°C)$^{-1}$ for MLD. The colored areas in (b–d) and (f–h) are statistically significant at the 99% confidence level.

variability is extracted using empirical orthogonal functions (EOF) analysis. Then, SST spatial patterns and corresponding temporal coefficients are obtained from EOF1 (observed variance contribution is approximately 42%; variance contribution simulated by GFDL-ESM2M is approximately 38%), which primarily represent the interannual pattern of SST associated with ENSO. Using the first principal component (PC1) of SSTA, we obtain the spatial distribution of some related fields using the regression analysis, including SSS, MLD and Q_B.

The first spatial pattern of SST extracted using EOF analysis and the relevant regression spatial patterns for various anomalous fields in observations are shown in Fig. 4. For example, during El Niño, a positive SST anomaly appears in the east-central basin (Fig. 4a), accompanied by a large positive FWF anomaly in the west-central basin of the Pacific, SPCZ, and ITCZ (Fig. 4b). The direct effect the positive FWF anomaly is to strengthen a negative SSS anomaly (Fig. 4c) in the west-central Pacific. Correspondingly, the surface ocean density becomes smaller, which tends to stabilize the upper ocean and depress the mixing at the base of the mixed layer. In addition, the MLD becomes shallower in the west-central equatorial Pacific (Fig. 4d), which also tends to suppress the entrainment of subsurface water into the mixed layer to enhance upper-ocean warming in the eastern Pacific. At the same time, the Q_S anomaly is positive in response to the positive FWF in the west-central basin (Fig. 5a). Thus, as part of Q_B, the positive Q_S anomaly acts to compensate for the negative Q_T anomaly (Fig. 5b), leading to a smaller negative Q_B anomaly (Fig. 5c). The reduced negative Q_B anomaly (i.e., due to the contribution of the positive Q_S anomaly) tends to decrease the MLD in the west-central equatorial region. These oceanic processes, which have been demonstrated by Zhang and Busalacchi (2009), are favorable for more warming in the surface layer.

Similar to the above observation, the SST EOF1 simulated by GFDL-ESM2M represents ENSO (Fig. 4e). Compared with the observation, there is a higher positive FWF anomaly into the ocean in the west-central equatorial Pacific (Fig. 4f), leading to a relatively stronger negative SSS anomaly (Fig. 4g) than that of the observed anomaly. The high volume of freshwater entering the ocean causes a low surface ocean density anomaly simulated by GFDL-ESM2M, renders the upper ocean more stable and weakens the mixing of the cold water into the mixed layer (Fig. 4h), which leads to stronger warming of SST during El Niño. As such, a warmer than observed SST is likely to be simulated by GFDL-ESM2M, as shown in Fig. 4e.

In addition, a stronger positive Q_S anomaly (Fig. 5d) is seen in the west-central basin and a negative Q_T anomaly (Fig. 5e) is seen in the east-central equatorial Pacific, compared with the observation. The positive FWF anomaly re-

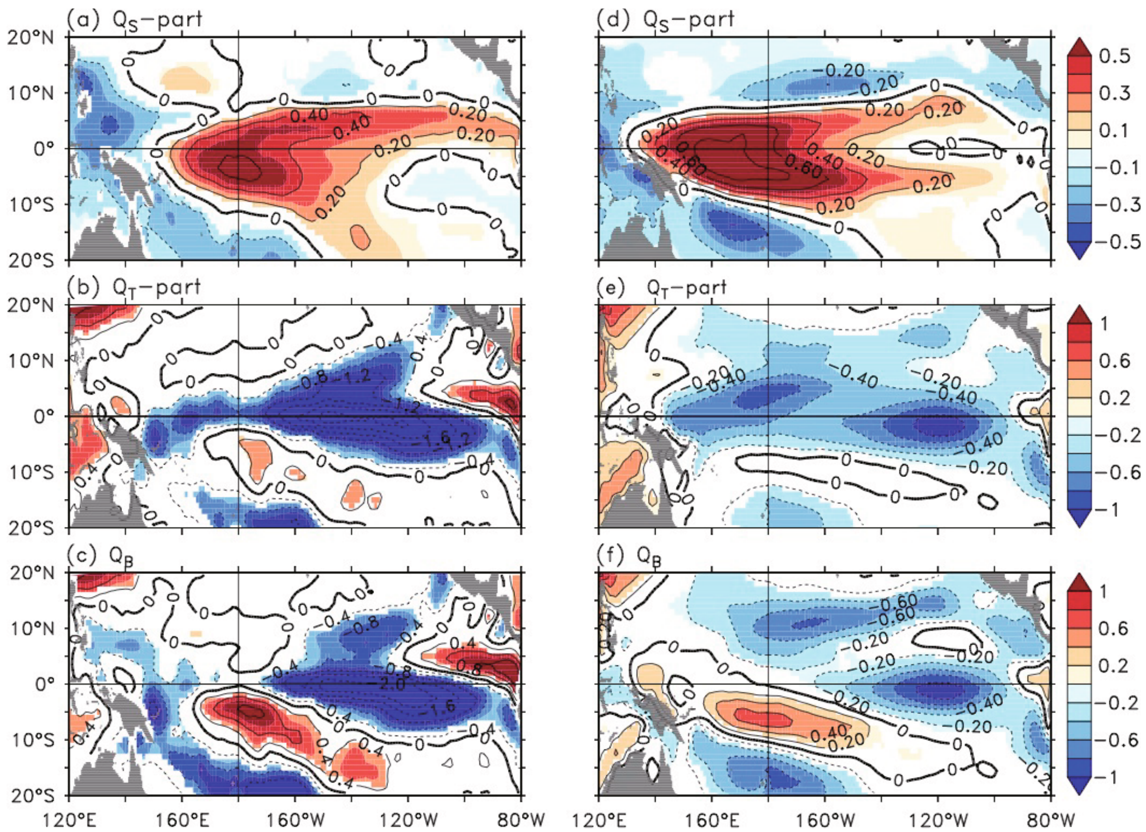

Fig. 5. The (a–c) observed and (d–f) GFDL-ESM2M simulated spatial patterns in the equatorial Pacific from SST PC1: (a, d) the Q_S part; (b, e) the Q_T part; (c, f) Q_B. The units are 1.0×10^{-5} kg m^{-2} s^{-1} (°C)$^{-1}$ for Q_S, Q_T and Q_B. The colored areas in (a–f) indicate where values are statistically significant at the 99% confidence level.

sults in a positive Q_S as part of the anomaly increases in the west-central equatorial Pacific, where Q_S makes the interannual Q_B a weaker negative anomaly (Fig. 5f), which makes the upper ocean more stable and thus depresses the mixing of cold water into the mixed layer. As such, the SST anomaly simulated by GFDL-ESM2M can be more positive than observed, as shown in Fig. 4e.

The above results can be considered as positive feedback between FWF and SST during ENSO cycles through the response of SSS, MLD and Q_B, because a stronger FWF anomaly simulated by GFDL-ESM2M leads to a stronger SSS anomaly in the west-central Pacific, and a stronger positive feedback to SST during El Niño is observed in the model results when compared with the observation. However, as exemplified by GFDL-ESM2M, the differences in FWFs simulated by the multi-model can exert striking differences in the modulation of SST in the equatorial Pacific; it is difficult to analyze a quantitative relationship based only on the spatial distribution of FWF, SSS and SST.

5. Correlation between FWF, SSS and SST, and related variability

In this section, based on the differences in the correlations among the FWF, SSS and SST interannual variabilities simulated by the multi-model and those observed, specific areas are selected to analyze the linear relationship. According to the distribution of interannual variability, FWF is selected from the box (2°S–2°N, 160°–180°E), SSS is selected from (2°S–2°N, 160°–180°E), and SST is selected from (2°S–2°N, 160°–160°W). Then, according to the regional averages of the three interannual variabilities indicated above, the quantifications of those linear relationships are analyzed. Table 2 shows that FWF interannual variability ranges from 1.0 to 5.2 mm d^{-1}, SSS is in the range of 0.08–0.8 psu, and the SST ranges from 0.8°C–1.96°C. As seen from the scatter plots, there are obvious linear relationships among the variables. For example, the FWF, SSS and SST variabilities averaged regionally in the results of BNU-ESM, FGOALS-s2 and HadGEM2-ES consistently correspond to larger variabilities, but those of CSIRO-MK3-6-0, MPI-ESM-LR and MRI-CGCM3 correspond to smaller values.

The corresponding relationships in the SST–FWF linear regression are analyzed according to the two pairs, SSS–FWF and SST–SSS. First, as shown in Fig. 6, the scattered distribution of FWF and SSS illustrates an obvious linear relationship simulated by the multi-model and based on observations. With the increase of FWF variability, the SSS increases in linearity, and the slope is 0.12 (Table 3). The physical mechanism responsible is that each 1 mm d^{-1} FWF anomaly can cause a 0.12 psu SSS anomaly in the tropical Pacific.

Similarly, Fig. 7 shows scatter plots for SSS and SST interannual variability, which can induce the linear relationship. For a slope of 0.93 (Table 3), it means that every 1.0 psu of SSS anomaly can bring about nearly 0.93°C of SST interannual change; therefore, SSS can be considered as a factor of

Table 2. List of the CMIP5 multi-models used to calculate the regional mean of SST, FWF and SSS STDs. The units are °C for SST, mm d^{-1} for FWF, and psu for SSS.

No.	Model name	SST (°C)	FWF (mm d^{-1})	SSS (psu)
1	ACCESS1-3	0.92	2.99	0.22
2	BNU-ESM	1.96	4.34	0.57
3	CCSM4	1.28	3.56	0.29
4	CESM1-CAM5	1.17	3.14	0.26
5	CMCC-CESM	1.66	4.67	0.62
6	CNRM-CM5	1.31	3.68	0.50
7	CSIRO-Mk3-6-0	0.85	1.45	0.26
8	CanESM2	1.25	2.69	0.12
9	FGOALS-g2	1.14	3.03	0.52
10	FGOALS-s2	1.51	3.35	0.80
11	GFDL-CM3	1.31	3.02	0.14
12	GFDL-ESM2G	0.99	1.12	0.08
13	GFDL-ESM2M	1.62	5.14	0.43
14	HadCM3	1.16	1.52	0.21
15	HadGEM2-ES	1.19	3.15	0.32
16	IPSL-CM5A-LR	0.91	1.021	0.10
17	IPSL-CM5A-MR	0.98	1.05	0.09
18	MIROC5	1.16	2.60	0.40
19	MPI-ESM-LR	0.91	1.06	0.09
20	MPI-ESM-P	1.02	1.50	0.12
21	MRI-CGCM3	0.83	2.86	0.39
22	NorESM1-M	1.33	3.62	0.34
23	bcc-csm1-1	1.20	4.65	0.24
24	Observation	0.99	3.22	0.36
	Mean	1.19	2.85	0.31

Note: SST box: 160°–120°W, 2.0°S–2.0°N
FWF box: 160°–180°E, 2.0°S–2.0°N
SSS box: 160°–180°E, 2.0°S–2.0°N

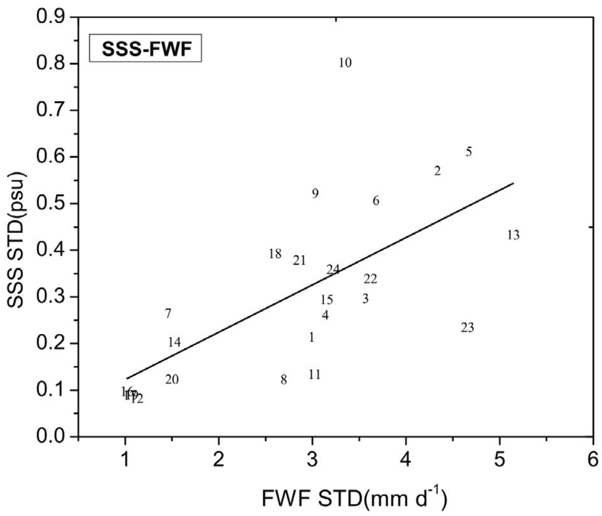

Fig. 6. Scatter plot of SSS STD and FWF STD in multi-model simulations and observations. Data points are the regional mean in the box (2.0°S–2.0°N, 160°–180°E). The line represents linear regression fits to the 23 CMIP5 models, and the 24th point is for observation (correlation coefficients r are shown in Table 3). The units are mm d^{-1} for FWF, and psu for SSS.

Table 3. List of the relevant coefficients of variation of the linear regressions for SST–FWF, SSS–FWF and SST–SSS.

	$a+bx$				
Function	a	b	R	STD	$P<0.001$
SST=F(FWF)	0.72 ± 0.10	0.11 ± 0.03	0.77	0.19	Y
SST=F(SSS)	0.90 ± 0.08	0.93 ± 0.24	0.68	0.21	Y
SSS=F(FWF)	0.03 ± 0.02	0.12 ± 0.03	0.675	0.15	Y

R: Correlation coefficient. STD: The standard deviation. $P<0.001$: 99.9% significance testing.

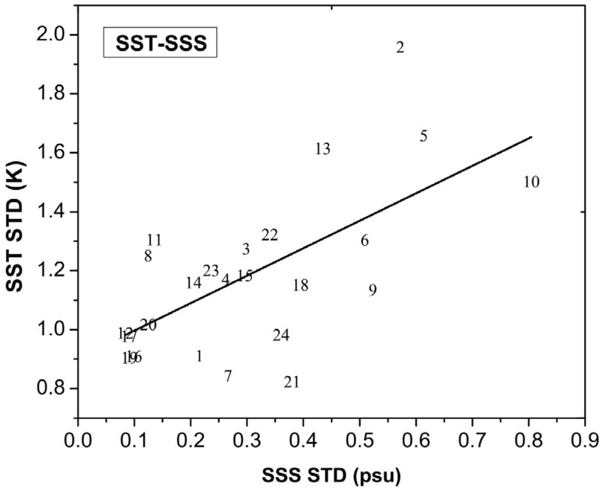

Fig. 7. Scatter plot of SST STD and SSS STD in multi-model simulations and observations. Data points are the regional mean of SST in the box (2.0°S–2.0°N, 160°–120°W) and SSS in the box (2.0°S–2.0°N, 160°–180°E). The line represents linear regression fits to the 23 CMIP5 models, and the 24th is for observation (correlation coefficients r are shown in Table 3). The units are °C for SST and psu for SSS.

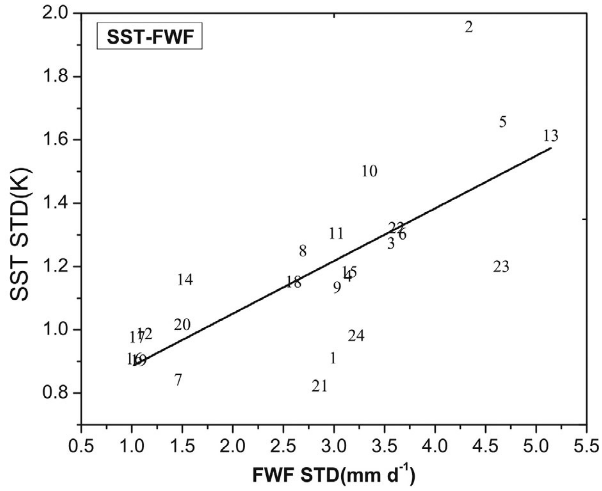

Fig. 8. Scatter plot of SST STD and FWF STD in multi-model simulations and observations. Data points are the regional mean of SST in the box (2.0°S–2.0°N, 160°–120°W) and FWF in the box (2.0°S–2.0°N, 160°–180°E). The line represents linear regression fits to 23 CMIP5 models, and the 24th point is for observation (correlation coefficients r are shown in Table 3). The units are °C for SST and mm d^{-1} for FWF.

positive influence on SST change.

The above analyses verify the interannual FWF modulations of SST in the equatorial Pacific through modulating SSS interannual anomalies. Furthermore, we can also comprehensively analyze the linear relationship between FWF and SST interannual anomalies (Fig. 8). A linear regression equation is derived for SST–FWF based on the scatter plots for FWF and SST simulated by the multi-model and based on observations (Table 3). The slope of the equation is 0.11, which means that, every 1.0 mm d^{-1}, FWF can indirectly result in a 0.11°C SST change in the tropical Pacific.

The contributions of ocean fields to SST anomalies can be defined by one value based on a single-variable linear regression equation. As an example of observed SST interannual variability in a regression equation, an FWF change of 3.22 mm d^{-1} can result in a 0.35°C SST anomaly (3.22 mm d^{-1} multiplied by 0.11). For 0.99 °C of SST average anomalies, the contribution rate of FWF to SST interannual anomalies is nearly 36% (0.35/0.99). Similarly, the FWF contribution rate to SST interannual anomalies can be derived from the CMIP5 multi-model, and we can generalize a conclusion from the facts that FWF interannual anomalies in the western equatorial Pacific can lead to approximately 12%–40% SST anomalies in the eastern equatorial Pacific, with a mean contribution rate of 24%.

6. Summary and conclusion

Although many studies have been conducted to investigate the effect and modulation of FWF and relevant salinity on SST in the tropical Pacific through diagnosis of observations and simulations, considerable uncertainty remains in determining clear linear relationships of the FWF effect on SSS and SST. Quantifying the direct influence of FWF on SSS, and the FWF modulation of SST in the equatorial Pacific, not only promotes the effectiveness of the model simulation of ocean fields but also helps to better predict SST interannual anomalies. This paper quantifies the linear relationship of the positive feedback of FWF to SST using the simulations of the CMIP5 multi-model and observations. The key conclusions can be summarized as follows:

(1) The interannual FWF variability in the western equatorial Pacific influences interannual SSS variability directly, and modulates SST in the eastern equatorial Pacific. When comparing the spatial distribution characteristics of FWF and related SSS and SST variability simulated by the CMIP5 multi-model and based on observations, it is found that a large FWF variability is located in the western equatorial Pacific, and the displacement of larger variability simulated by most models moves eastward across the date line and increases SSS in the western equatorial Pacific to warm SST in the eastern equatorial Pacific. CMIP5 multi-models can re-

produce the ocean processes observed, but the simulation capabilities of the multi-models are different with regard to the magnitude and position of FWF and related SSS and SST.

(2) The differences in model intrinsic properties among multi-models may lead to an inconsistent feedback effect on oceanic fields. Based on the intensities and positions of the positive feedback to SST, GFDL-ESM2M is selected from among the CMIP5 multi-model simulations to analyze the differences in ocean physical processes with respect to FWF feedback to SST in the equatorial Pacific. The fact that the interannual FWF variability simulated by GFDL-ESM2M is stronger than observed can lead to a larger negative SSS anomaly and a more negative ML anomaly in the western equatorial Pacific. In other words, the stronger FWF can cause $Q_{\rm S}$ to compensate for the $Q_{\rm B}$ more effectively. The less negative $Q_{\rm B}$ anomaly and shallower MLD create more positive feedback to an SST anomaly to warm the upper ocean. Differences in FWF in the western Pacific lead to the differences in ocean physical processes among the models and observations, such that the feedback to SST is highly sensitive to FWF and related ocean fields in the equatorial Pacific.

(3) Simple linear relationships exist in the interannual variability of FWF, SSS and SST. There are positive linear relationships among the interannual variabilities of FWF with SSS, SSS with SST, and FWF with SST. Based on the slopes of linear regression equations, an FWF anomaly of 1.0 mm d^{-1} causes an SSS anomaly of nearly 0.12 psu in the tropical Pacific, and a 1.0 psu SSS anomaly leads to an SST anomaly of 0.93°C. In general, a 1.0 mm d^{-1} FWF anomaly indirectly corresponds to a 0.11°C SST anomaly.

Acknowledgements. We thank the modeling groups participating in CMIP5, and PCMDI, for generously making their output available. This study was supported by the National Natural Science Foundation of China (NSFC) (Grant Nos. 41376039, 41376019 and 41475101), the NSFC–Shandong Joint Fund for Marine Science Research Centers (Grant No. U1406401), the NSFC Innovative Group Grant (Project No. 41421005), and the Institute of Oceanology, Chinese Academy of Sciences (IOCAS) through the Chinese Academy of Sciences Strategic Priority Project [the Western Pacific Ocean System (WPOS)]. This is publication No. 047 of the Earth System Modeling Center, supported by the Joint Center for Global Change Studies (Project No. 105019), and the Priority Academic Program Development (PAPD) of Jiangsu Higher Education Institutions.

REFERENCES

Adler, R. F., and Coauthors, 2003: The version-2 global precipitation climatology project (GPCP) monthly precipitation analysis (1979–present). *Journal of Hydrometeorology*, **4**(6), 1147–1167.

Ballabrera-Poy, J., R. Murtugudde, R.-H. Zhang, and A. J. Busalacchi, 2007: Coupled ocean-atmosphere response to seasonal modulation of ocean color: Impact on interannual climate simulations in the tropical Pacific. *J. Climate*, **20**, 353–374.

Bao, Q., and Coauthors, 2013: The flexible global ocean–atmosphere–land system model, spectral version 2: FGOALS-s2. *Adv. Atmos. Sci.*, **30**, 561–576, doi: 10.1007/s00376-012-2113-9.

Bentsen, M., and Coauthors, 2012: The Norwegian Earth System Model, NorESM1-M-Part 1: Description and basic evaluation of the physical climate. *Geoscientific Model Development*, **6**, 687–720.

Béthoux, J.-P., B. Gentili, and D. Tailliez, 1998: Warming and freshwater budget change in the Mediterranean since the 1940s, their possible relation to the greenhouse effect. *Geophys. Res. Lett.*, **25**, 1023–1026.

Bjerknes, J., 1969: Atmospheric teleconnections from the equatorial Pacific. *Mon. Wea. Rev.*, **97**, 163–172.

Boyer, T. P., S. Levitus, J. I. Antonov, R. A. Locarnini, and H. E. Garcia, 2005: Linear trends in salinity for the World Ocean, 1955–1998. *Geophys. Res. Lett.*, **32**, L01604, doi: 10.1029/2004GL021791.

Collins, M, S. F. B. Tett, and C. Cooper, 2001: The internal climate variability of HadCM3, a version of the Hadley Centre coupled model without flux adjustments. *Climate Dyn.*, **17**(1), 61–81.

Collins, M., and Coauthors, 2010: The impact of global warming on the tropical Pacific Ocean and El Niño. *Nature Geoscience*, **3**(6), 391–397.

Cravatte, S., T. Delcroix, D. X. Zhang, M. McPhaden, and J. Leloup, 2009: Observed freshening of the warming western tropical Pacific and extension of the Warm/Fresh pool in recent decades. *Climate Dyn.*, **33**, 565–589, doi: 10.1007/s00382-009-0526-7.

Curry, R., B. Dickson, and I. Yashayaev, 2003: A change in the freshwater balance of the Atlantic Ocean over the past four decades. *Nature*, **426**, 826–829.

Danabasoglu, G., S. C. Bates, B. P. Briegleb, S. R. Jayne, M. Jochum, W. G. Large, S. Peacock, and S. G. Yeager, 2012: The CCSM4 ocean component. *J. Climate*, **25**(5), 1361–1389.

Delcroix, T., and C. Hénin, 1991: Seasonal and interannual variations of sea surface salinity in the tropical Pacific Ocean. *J. Geophys. Res.*, **96**(C12), 22 135–22 150.

Dickson, B., I. Yashayaev, J. Meincke, B. Turrell, S. Dye, and J. Holfort, 2002: Rapid freshening of the deep North Atlantic Ocean over the past four decades. *Nature*, **416**, 832–837.

Dix, M., and Coauthors, 2013: The ACCESS coupled model: Documentation of core CMIP5 simulations and initial results. *Australian Meteorological and Oceanographic Journal*, **63**(1), 83–99.

Dufresne, J.-L., and Coauthors, 2013: Climate change projections using the IPSL-CM5 Earth System Model: From CMIP3 to CMIP5. *Climate Dyn.*, **40**, 2123–2165.

Dunne, J. P., and Coauthors, 2013: GFDL's ESM2 global coupled climate-carbon earth system models. Part II: Carbon system formulation and baseline simulation characteristics. *J. Climate*, **26**, 2247–2267.

Fedorov, A. V., R. C. Picanowski, S. G. Philander, and G. Boccaletti, 2004: The effect of salinity on the wind-driven circulation and the thermal structure of the upper ocean. *J. Phys. Oceanogr.*, **34**, 1949–1966.

Giorgetta, M. A., and Coauthors, 2013: Climate and carbon cycle changes from 1850 to 2100 in MPI-ESM simulations for the Coupled Model Intercomparison Project phase 5. *Journal of Advances in Modeling Earth Systems*, **5**(3), 572–597.

Griffies, S. M., and Coauthors, 2011: The GFDL CM3 coupled climate model: Characteristics of the ocean and sea ice simulations. *J. Climate*, **24**, 3520–3544.

Hackert, E., J. Ballabrera-Poy, A. J. Busalacchi, R.-H. Zhang, and R. Murtugudde, 2011: Impact of sea surface salinity assimilation on coupled forecasts in the tropical Pacific. *J. Geophys. Res.*, **116**, C05009, doi: 10.1029/2010JC006708.

Ham, S., S.-Y. Hong, Y. Noh, S. I. An, Y.-H. Byun, H.-S. Kang, J. Lee, and W.-T. Kwon, 2012: Effects of freshwater runoff on a tropical pacific climate in the HadGEM2. *Asia-Pacific Journal of Atmospheric Sciences*, **48**(4), 457–463.

Huang, B. Y., and V. M. Mehta, 2005: Response of the Pacific and Atlantic oceans to interannual variations in net atmospheric freshwater. *J. Geophys. Res.*, **110**, C08008, doi: 10.1029/2004JC002830.

Huang, B. Y., V. M. Mehta, and N. Schneider, 2005: Oceanic response to idealized net atmospheric freshwater in the Pacific at the decadal time scale. *J. Phys. Oceanogr.*, **35**, 2467–2486.

Ingleby, B., and M. Huddleston, 2007: Quality control of ocean temperature and salinity profiles–historical and real-time data. *J. Mar. Syst.*, **65**, 158–175.

Iversen, T., and Coauthors, 2012: The Norwegian Earth System Model, NorESM1-M —Part 2: Climate response and scenario projections. *Geoscientific Model Development*, **6**, 389–415.

Jacobs, S. S., C. F. Giulivi, and P. A. Mele, 2002: Freshening of the Ross Sea during the late 20th century. *Science*, **297**,386–389.

Jeffrey, S, L. Rotstayn, M. Collier, S. Dravitzki, C. Hamalainen, C. Moeseneder, K. Wong, and J. Syktus, 2013: Australia's CMIP5 submission using the CSIRO–Mk3. 6 model. *Australian Meteorological and Oceanographic Journal*, **63**, 1–13.

Ji, D., and Coauthors, 2014: Description and basic evaluation of BNU-ESM version1. *Geoscientific Model Development*, **7**, 1601–1647.

Jones, C. D., and Coauthors, 2011: The HadGEM2-ES implementation of CMIP5 centennial simulations. *Geoscientific Model Development*, **4**, 543–570.

Kang, X. B., R. H. Huang, Z. G. Wang, and R.-H. Zhang, 2014: Sensitivity of ENSO variability to Pacific freshwater flux adjustment in the Community Earth System Model. *Adv. Atmos. Sci.*, **31**(5), 1009–1021, doi: 10.1007/s00376-014-3232-2.

Kim, S.-B., T. Lee, and I. Fukumori, 2007: Mechanisms controlling the interannual variation of mixed layer temperature averaged over the Niño-3 region. *J. Climate*, **20**, 3822–3843.

Lagerloef, G. S. E., 2002: Introduction to the special section: The role of surface salinity on upper ocean dynamics, air-sea interaction and climate. *J. Geophys. Res.*, **107**(C12), SRF 1-1–SRF 1-2, doi: 10.1029/2002JC001669.

Levitus, S., 1989: Interpentadal variability of temperature and salinity at intermediate depths of the North Atlantic Ocean, 1970–1974 versus 1955–1959. *J. Geophys. Res.*, **94**(C5), 6091–6131.

Levitus, S., J. I. Antonov, T. P. Boyer, H. E. Garcia, and R. A. Locarnini, 2005: Linear trends of zonally averaged thermosteric, halosteric, and total steric sea level for individual ocean basins and the world ocean, (1955–1959) versus (1994–1998). *Geophys. Res. Lett.*, **32**, L16601, doi: 10.1029/2005GL023761.

Li, L. J., and Coauthors, 2013: The flexible global ocean-atmosphere-land system model, Grid-point Version 2: FGOALS-g2. *Adv. Atmos. Sci.*, **30**, 543–560, doi: 10.1007/s00376-012-2140-6.

Ma, H., L. X. Wu, and Z. Q. Li, 2013: Impact of freshening over the Southern Ocean on ENSO. *Atmospheric Science Letters*, **14**(1), 28–33.

Maes, C., 1998: Estimating the influence of salinity on sea level anomaly in the ocean. *Geophys. Res. Lett.*, **25**, 3551–3554.

Maes, C., 2000: Salinity variability in the equatorial Pacific Ocean during the 1993–98 period. *Geophys. Res. Lett.*, **27**, 1659–1662.

Manabe, S., and R. J. Stouffer, 1995: Simulation of abrupt climate change induced by freshwater input to the North Atlantic Ocean. *Nature*, **378**, 165–167.

Meehl, G. A., P. R. Gent, J. M. Arblaster, B. L. Otto-Bliesner, E. C. Brady, and A. Craig, 2001: Factors that affect the amplitude of El Niño in global coupled climate models. *Climate Dyn.*, **17**, 515–526.

Meehl, G. A., and Coauthors, 2013: Climate change projections in CESM1 (CAM5) compared to CCSM4. *J. Climate*, **26**, 6287–6308.

Schiffer, R. A., and W. B. Rossow, 1985: ISCCP global radiance data set: A new resource for climate research. *Bull. Amer. Meteor. Soc.*, **66**(12), 1498–1505.

Smith, T. M., R. W. Reynolds, T. C. Peterson, and J. Lawrimore, 2008: Improvements to NOAA's historical merged land-ocean temp analysis (1880–2006). *J. Climate*, **21**, 2283–2296.

Taylor, K. E., R. J. Stouffer, and G. A. Meehl, 2012: An overview of CMIP5 and the experiment design. *Bull. Amer. Meteor. Soc.*, **93**(4), 485–498.

Voldoire, A., and Coauthors, 2013: The CNRM-CM5. 1 global climate model: Description and basic evaluation. *Climate Dyn.*, **40**(9–10), 2091–2121.

Watanabe, M., and Coauthors, 2010: Improved climate simulation by MIROC5: Mean states, variability, and climate sensitivity. *J. Climate*, **23**(23), 6312–6335.

Wong, A., N. Bindoff, and J. Church, 1999: Large-scale freshening of intermediate waters in the Pacific and Indian Oceans. *Nature*, **400**, 440–443.

Wong, A. P. S., N. L. Bindoff, and J. A. Church, 2001: Freshwater and heat changes in the north and south Pacific Oceans between the 1960s and 1985–94. *J. Climate*, **14**, 1613–1633.

Wu, L. X., Y. Sun, J. X. Zhang, L. P. Zhang, and S. Minobe, 2010: Coupled ocean-atmosphere response to idealized freshwater forcing over the Western Tropical Pacific. *J. Climate*, **23**(7), 1945–1954.

Wu, T., and Coauthors, 2014: An overview of BCC climate system model development and application for climate change studies. *J. Meteor. Res.*, **28**(1), 34–56.

Yu, B., and G. Boer, 2002: The roles of radiation and dynamical processes in the El Niño-like response to global warming. *Climate Dyn.*, **19**, 539–553.

Yu, L. S., and R. A. Weller, 2007: Objectively analyzed air-sea heat fluxes for the global ice-free oceans (1981–2005). *Bull. Amer. Meteor. Soc.*, **88**, 527–539.

Yukimoto, S., and Coauthors, 2012: A new global climate model of the meteorological research institute: MRI-CGCM3-model description and basic performance. *J. Meteor. Soc. Japan.*, **90A**, 23–64.

Zhang, L. P., C. Z. Wang, and S.-K. Lee, 2014: Potential role of Atlantic Warm Pool-induced freshwater forcing in the Atlantic Meridional Overturning Circulation: Ocean-sea ice model simulations. *Climate Dyn.*, **43**, 553–574.

Zhang, R.-H., and A. J. Busalacchi, 2009: Freshwater flux (FWF)-induced oceanic feedback in a hybrid coupled model of the tropical Pacific. *J. Climate*, **22**, 853–879.

Zhang, R.-H., G. H. Wang, D. K. Chen, A. J. Busalacchi, and E. C.

Hackert, 2010: Interannual biases induced by freshwater flux and coupled feedback in the tropical pacific. *Mon. Wea. Rev.*, **138**, 1715–1737.

Zhang, R.-H., F. Zheng, J. S. Zhu, Y. H. Pei, Q. A. Zheng, and Z. G. Wang, 2012: Modulation of El Niño-Southern Oscillation by freshwater flux and salinity variability in the tropical Pacific. *Adv. Atmos. Sci.*, **29**(4), 647–660, doi: 10.1007/s00376-012-1235-4.

Zhang, R.-H., F. Zheng, J. Zhu, and Z. G. Wang, 2013: A successful real-time forecast of the 2010–11 La Niña event. *Scientific Reports*, **3**, 1108, doi: 10.1038/srep01108.

Zheng, F., and R.-H. Zhang, 2012: Effects of interannual salinity variability and freshwater flux forcing on the development of the 2007/08 La Niña event diagnosed from Argo and satellite data. *Dyn. Atmos. Oceans*, **57**, 45–57.

Zheng, F., R.-H. Zhang, and J. Zhu, 2014: Effects of interannual salinity variability on the barrier layer in the western-central equatorial Pacific: A diagnostic analysis from Argo. *Adv. Atmos. Sci.*, **31**(3), 532–542, doi: 10.1007/s00376-013-3061-8.